Electrolyte Stability in a Nanochannel with Charge Regulation

Cédric Beaume,*,† Franck Plouraboué,† Alain Bergeon,† and Edgar Knobloch‡

†Université de Toulouse, INP, and CNRS, IMFT (Institut de Mécanique des Fluides de Toulouse), Allée Camille Soula, F-31400 Toulouse, France

‡Department of Physics, University of California, Berkeley, California 94720, United States

ABSTRACT: The stability of an electrolyte confined in one dimension between two solid surfaces is analyzed theoretically in the case where overlapping double layers produce nontrivial interactions. Within the Poisson−Boltzmann−Nernst−Planck description of the electrostatic interaction and transport of electrical charges, the presence of Stern layers can enrich the set of possible solutions. Our analytical and numerical study of the stability properties of the trivial state of this system identified an instability to a new antisymmetric state. This state is stable for a range of gap widths that depends on the Debye and Stern lengths, but for smaller gap widths, where the Stern layers overlap, a second transition takes place and the stable nontrivial solution diverges. The origin of this divergence is explained and its properties analyzed using asymptotic techniques which are in good agreement with numerical results. The relevance of our results to confined electrolytes at nanometer scales is discussed in the context of energy storage in nanometric systems.

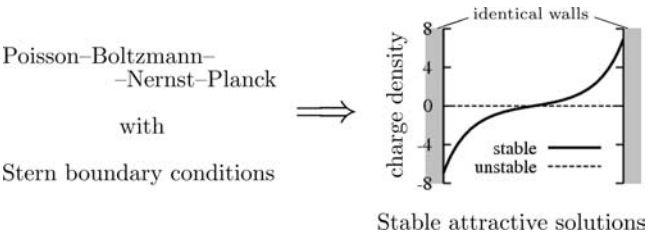

1. INTRODUCTION

The advent of integrated electrokinetic systems has renewed interest in employing such systems for manipulation of small-scale flows of charged liquids using electrical forces. Electrokinetic effects increase within decreasing scale and are therefore especially important when a charged liquid is confined to small domains. The stability of electro-osmotic flows confined between parallel plates has been investigated in several recent papers motivated by mesoscale experimental observations of flow instability.[1,2] Far from double layers, at a scale much larger than the Debye length, charged electrolytes are almost electroneutral and diffusive currents are negligible compared to electromigration. The resulting "ohmic" model approximation for the electrolyte is commonly used[3,4] for analyzing the dynamics of electrokinetic flows. In this framework, the presence of electrolyte concentration gradients induces electrical conductivity changes which are in turn responsible for electrical potential variations.[5,6] Abrupt electrolyte concentration variations can induce both longitudinal and transverse variations in the potential leading to flow instability.[5,6]

When convective transport dominates over diffusive (the large Péclet number regime), a recent study[7] shows that the electrokinetic flow is stable even in the presence of time-dependent electrical forcing. In this case, the nonstationary flow in the Stokes layers near the boundaries decouples from the bulk electrokinetic problem, but is driven by the Coulomb forces arising in the bulk. These studies have been restricted to the linear Debye−Hückel approximation and are all based on the thin double-layer approximation. In this limit, the bulk electrolyte remains quasi-neutral, and the double layer remains in thermal quasi-equilibrium. However, dynamical studies investigating the stability at the double-layer scale have apparently not been done. At this scale, charges are no longer locally electroneutral, and nonlinearities involving the potential and ion concentration can play an important role.

At these very small scales, the electrokinetic phenomenon involves new physical effects that are still not clearly elucidated. For example, dynamical charge relaxation involves a very fast time scale associated with various diffusion times across the double layer.[8] At distances on the order of the Debye length, when the electrolyte is confined between two solid surfaces, the double layers overlap and their interaction can produce nontrivial attraction[9,10] and ion concentration profile.[11] This is not true for imposed surface charges, where Poisson−Boltzmann electrostatic interactions are always repulsive,[12] unless nonsymmetric boundary conditions associated with nonidentical surfaces are considered.[13,14]

However, attraction can occur even for symmetric boundary conditions provided charge regulation is included, as first noted in refs 15,16 and subsequently analyzed in ref 9. In other situations charge regulation produces repulsion.[17] In the present work, we concentrate on "reduced" charge regulation for which the surface charge *decreases* with the applied electrical potential, in contrast to the case studied in ref 8. In this case, Stern layers associated with mixed boundary conditions for the electrical potential destabilize the trivial state, leading to a nontrivial symmetry-breaking stationary solution describing attractive interaction between solid surfaces.[9] Such Stern layers are consistent with modified mean-field descriptions incorporating fluctuations and charge correlation effects.[9,18] Interest in this specific case is justified within the framework of Langmuir and Frumkin−Fowler−Guggenheim (FFG) mass action models as

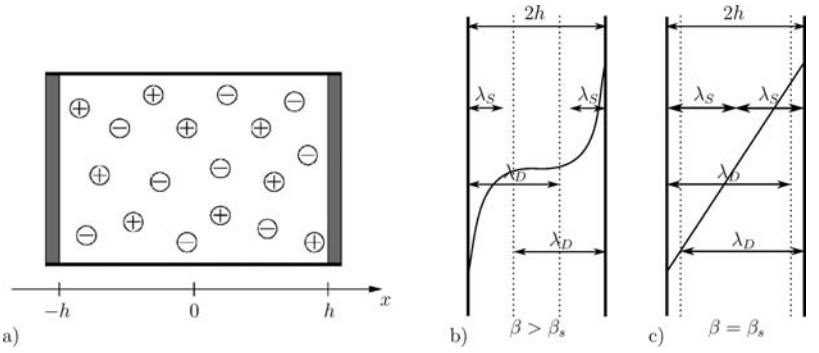

Figure 1. (a) Sketch of the system with a neutral monovalent electrolyte confined between two chargeable walls located at $x = \pm h$. The Debye and Stern lengths λ_D and λ_S relative to the gap width $2h$ when (b) $\beta > \beta_s$ and (c) $\beta = \beta_s$. The corresponding electrical potential $\phi(x)$ is superposed.

discussed in section 2.1.3. In ref 9, the attractive far-field behavior of "reduced" charge regulation solutions between similar surfaces was successfully compared with atomic force microscopy measurements obtained in ref 19. The present contribution analyzes in greater depth the origin of such attractive solutions, as well as their stability properties with respect to parameter changes including charge density variations and potential disturbances. In the context of charge transport balance formulation, the study shows that attractive solutions are not only robust but also display a dramatic increase in the wall potential at small separations, similar to that observed in refs 20,21 that can swamp the spring constant of an AFM probe tip at small distances. It is important, therefore, to also consider the stability properties of both the trivial and nontrivial solutions, and to do so within the framework of a Poisson−Nernst−Planck mean-field description.

The problem is formulated in section 2 together with the governing equations and a brief summary of the numerical method used to solve them. The linear stability of the trivial homogeneous solution of the Poisson−Nernst−Planck equations is studied analytically in section 3. Section 4 is devoted to a description of the numerical results and an analytical treatment of the behavior of the system near a singularity identified in the course of the numerical study. Two cases are studied, with and without an imposed electric field, focusing on a closed system with a fixed number of charges. In section 4.3, we consider the effects of different diffusivities of the anions and cations; in section 4.4, the case of a non electroneutral electrolyte is briefly described; the influence of the different Stern layers is discussed in section 4.5. Brief discussion and conclusions follow in section 5.

2. CONSTITUTIVE EQUATIONS AND NUMERICAL METHOD

2.1. Governing Equations. *2.1.1. Dimensionless Formulation.* We consider a neutral monovalent electrolyte between two chargeable, planar, and parallel vertical walls, as in Figure 1. In the case considered here, the vertical extent of the walls is sufficiently large compared to the gap $2h$ that a one-dimensional formulation is appropriate, and we use the variable x to refer to the horizontal coordinate transverse to the walls. The electrolyte is taken to consist of dissociated cations and anions with identical mobilities and diffusivities, satisfying the Poisson equation

$$\varepsilon\varepsilon_0 \nabla\cdot\mathbf{E} = e(c^+ - c^-) \tag{1}$$

Here, ε is the electrolyte permittivity, ε_0 the vacuum permittivity, e the elementary electrical charge, c^+ and c^- are, respectively, the cation and the anion number densities, and $\mathbf{E}$ is the electric field that may be written as the gradient of a potential ϕ

$$\mathbf{E} = -\nabla\phi \tag{2}$$

defined to within a constant. The diffuse-charge dynamics are described by the Nernst−Planck equations

$$\partial_t c^\pm = \partial_x(D\partial_x c^\pm \pm \mu c^\pm \partial_x\phi) \tag{3}$$

where t is the time, D is the (constant) ion diffusivity, and μ is the (constant) ion mobility given by the Einstein-Smoluchowski formula

$$\mu = \frac{De}{k_B T} \tag{4}$$

Here, k_B is the Boltzmann constant and T is the temperature. As already mentioned, we assume that the diffusivities of positive and negative charges are identical. However, it is important to stress that when we relax this hypothesis (see section 4.3) we find that doubly diffusive effects do not qualitatively affect the conclusions reached with a single diffusivity hypothesis. Finally, it is also interesting to mention that we have neglected convective transport contribution in eq 3 because, at nanometer scale, diffusive transport is generally much faster than convection (zero Péclet number limit).

In the following, lengths, time, and the number densities $c^\pm$ are nondimensionalized, respectively, using half the wall separation h, the diffusive time scale $\tau \equiv h^2/D$, and the number density c_0 of cations in the absence of an electric field (equivalently, anions, since both of these constants are equal, owing to electroneutrality and isovalence). The electrical potential ϕ is nondimensionalized by $k_B T/e$. The dimensionless Poisson−Nernst−Planck equations read

$$\Delta\phi = \frac{\beta}{2}(c^- - c^+) \tag{5}$$

$$\partial_t c^+ = \partial_x(\partial_x c^+ + c^+\partial_x\phi) \tag{6}$$

$$\partial_t c^- = \partial_x(\partial_x c^- - c^-\partial_x\phi) \tag{7}$$

and are *time-dependent*. Here, $\Delta \equiv \partial^2_{xx}$ and the variables x, t, $c^\pm$, and ϕ now refer to dimensionless quantities. In the following, we refer to $c^\pm$ as *concentrations*; number densities can be converted to true or relative concentrations by dividing by the Avogadro number Av or by a reference number density such as c_0, but these prefactors cancel out from the above equations. In eq 5, the parameter $\beta \equiv h^2/\lambda_D^2$

quantifies the relation between the gap width $2h$ and the Debye length λ_D defined by

$$\lambda_D = \sqrt{\frac{\varepsilon\varepsilon_0 k_B T}{2e^2 c_0}} \tag{8}$$

In the following, we shall be interested in the case of overlapping double layers corresponding to the case $\beta < 1$ (see Figure 1). Following classical formulation,[22] we introduce the total concentration $c \equiv c^+ + c^-$ and the charge density $\rho \equiv c^+ - c^-$ and rewrite eqs 5−7 in the form

$$\Delta\phi = -\frac{\beta}{2}\rho \tag{9}$$

$$\partial_t c = \partial_x(\partial_x c + \rho\partial_x\phi) \tag{10}$$

$$\partial_t \rho = \partial_x(\partial_x \rho + c\partial_x\phi) \tag{11}$$

We assume that the flux of anions and cations across the boundaries vanishes

$$\partial_x c + \rho\partial_x\phi = \partial_x\rho + c\partial_x\phi = 0 \quad \text{at} \quad x = \pm 1 \tag{12}$$

Under these conditions, eqs 10 and 11 show that $\partial_t\langle c\rangle = \partial_t\langle\rho\rangle = 0$, where $\langle f\rangle = \int_{-1}^{1} f\,dx$. Thus, the number of anions and cations in the electrolyte remains constant in time. To fix these constants, we take the global charge of the electrolyte to be zero corresponding to an electrically neutral system. In dimensionless form, this assumption leads to the constraints

$$\langle c\rangle - 2\bar{c} = \langle\rho\rangle = 0 \tag{13}$$

where $\bar{c}$ is a constant determined by the number density of anions and cations prior to charge separation. This condition preserves global charge neutrality in the bulk plus solution. For simplicity, we consider first an electrolyte with identical anion and cation diffusivities, with global charge neutrality, i.e., $\langle\rho\rangle \equiv \bar{\rho} = 0$, and no applied electric field. Our conclusions extend, however, to the more general case of an applied electric field (as shown in section 4.2), heterogeneous ion properties (as shown in section 4.3), and non-electroneutral liquid bulk for which $\bar{\rho} \neq 0$ (as shown in section 4.4).

In view of our nondimensionalization, we take $\bar{c} = 2$, although our analytical calculations are carried out for general $\bar{c}$. In some applications, for example, in open systems in which the system is in contact with electrolyte reservoirs above and below, $\bar{c}$ can be a function of z, the coordinate parallel to the walls.[11]

2.1.2. Stern Layer Boundary Conditions. It remains to specify the boundary conditions on the electrical potential ϕ at the solid surfaces. The appropriate conditions go back to the work of O. Z. Stern,[23] albeit with a physical interpretation that benefits from recent advances in statistical fluctuation theory analysis of surface adsorption.[9,18] This analysis modifies the traditional physical picture of the Stern boundary conditions (see, e.g., refs 24,25) and attributes to Stern layers chemical and entropic contributions to the charge regulation capacity, in addition to the traditional electrical contribution.[13] In the traditional picture, developed by Stern[23] and used in many subsequent studies, e.g., refs 24,25, a Stern layer (sometimes separated into an inner and an outer part[24]) is a region where transverse spatial variations of the potential are taken to be linear, with an apparent dielectric permittivity different from the double-layer bulk. The value of the electrical potential ϕ at the outer edge of the boundary layer which connects to the double layer is called ζ. In the context of a thin double layer, the Stern layer is sometimes considered as providing an effective boundary condition to capture the compact counterion sublayer resulting from local Poisson−Boltzmann equilibrium. This point of view is not supported by fluctuation theory[9,18] where charge regulation is the result of local surface−bulk interactions, at a scale smaller than the Debye length. Such a local picture of the Stern layer is also supported by mass action models in which the local Stern surface charge/field relation results from adsorption/desorption kinetics, independent of the Debye scale. This is the reason charge regulation boundary conditions can be applied even on the scale of overlapping double layers.[26] Nonetheless, the fact remains that in the case of overlapping thick double layers with charge regulation boundary conditions the local electrical potential on one wall depends on the potential on the other, resulting in an indirect coupling between the two.

The linear variation of the potential with transverse coordinate within the Stern layer is described through the ratio of two parameters σ_d/C, the surface charge density σ_d divided by the Stern layer capacitance C. From Gauss' theorem, the surface charge density is proportional to the transverse electric field at the double-layer edge and the double-layer bulk permittivity ε, $\sigma_d \sim -\varepsilon\, d\phi/dx$, with a negative sign in the presence of negative surface charges and no adsorbed counterions.[25] The Stern layer capacitance C is proportional to the Stern layer permittivity ε_r and inversely proportional to the Stern layer width λ_S, $C \sim \varepsilon_r/\lambda_S$. In this picture, valid at each solid boundary, the Stern boundary condition thus reads

$$\phi = \zeta - \frac{\sigma_d}{C} \equiv \zeta + \frac{\varepsilon\lambda_S}{\varepsilon_r}\frac{\partial\phi}{\partial x} \tag{14}$$

Thus

$$\frac{\partial\phi}{\partial x} = \frac{\varepsilon_r}{\varepsilon\lambda_S}(\phi - \zeta) \tag{15}$$

A more up-to-date picture of the boundary condition eq 15 emerges from analyzing the electrical, chemical, and entropic contributions to charge regulation within a statistical mechanics framework. These lead to a modified mean-field Poisson−Boltzmann equations with surface source terms.[18] In the weak-field regime, these surface terms can in turn be mapped into a Stern layer type boundary condition eq 15.[9] Moreover, when the Stern layer permittivity is taken to equal the bulk permittivity, this mapping provides an explicit formula for the Stern layer width in terms of intrinsic constitutive parameters such as the Bjerrum length ℓ_B, the ionic charge number Z, and the surface charge density n_c of condensed ions, viz., $\lambda_S = 1/\pi Z^2 \ell_B n_c$.[9] In fact, as discussed in refs 3 and 9, boundary conditions of the *same* type result from a linearization of the adsorption isotherm potential/concentration, the sign of which depends on the specific kinetics.

A dimensionless formulation of the Stern layer boundary condition eq 15, with the half-gap h used as the length scale for transverse variation of ϕ, leads to the conditions

$$\partial_x\phi = \pm\nu\sqrt{\beta}(\phi - \phi_\pm) \quad \text{at} \quad x = \pm 1 \tag{16}$$

where $|\nu| \equiv \lambda_D/\lambda_S$ measures the width of the electrical double layer relative to the Stern layer width, and $\phi_\pm$ denotes the dimensionless ζ-potentials outside the Stern layers. These potentials may be zero or nonzero and of opposite signs as in the case of an applied transverse electric field (see below). In the

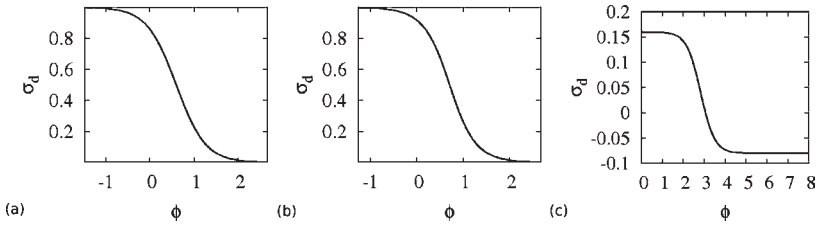

Figure 2. (a) and (b) Sketches of the adsoption isotherm from, respectively, the Langmuir and Frumkin−Fowler−Guggenheim models.[29] The parameters are $Z = 3$, $k_d^0/(k_a^0 C_b) = 1/6$ and (a) $\Delta G/RT = 0$, (b) $\Delta G/RT = -2$, as used in ref 29. (c) Sketch of the adsorption isotherm for cobalt-hexamine on silica surfaces as given by eq 21.[19] In each figure, σ_d represents the surface charge density and ϕ is the applied electrical potential.

following, we shall be interested in the case $\lambda_S < h$ depicted in Figure 1, corresponding to $1/\nu^2 < \beta < 1$.

The sign of the parameter ν has important consequences for the stability properties of the basic state. As already mentioned, previous derivations led to the estimate $\nu \sim \lambda_D/\ell_B n_c$, with a positive prefactor, implying that $\nu > 0$. This result is consistent with fluctuation theory-based modified mean-field equations.[18] However, the sign in the Stern layer mixed boundary condition depends on the dependence of σ_d on the potential. In particular, when σ_d increases with ϕ the parameter ν is negative.[27] This case is studied in ref 8. In contrast, when σ_d decreases with ϕ the parameter ν is positive. In section 2.1.3, we discuss different mass action models which lead to the latter relationship, and conclude that both signs of ν arise in practice.

It should be mentioned that with the Bjerrum length ℓ_B = 0.7 nm at 300 K and the surface ion density n_c considered by Jiang and Stein,[28] i.e., 0 .5nm^{-2} < n_c < 5 nm^{-2}, the expression $\lambda_S = 1/\pi Z^2 \ell_B n_c$ shows that for monovalent ions ($Z = 1$) the Stern length λ_S falls in the range 0.9 nm < λ_S < 9 nm. Thus, the Stern length may represent a substantial fraction of the Debye length if the latter is smaller than 20 nm. In this case, the parameter $|\nu| \equiv \lambda_D/\lambda_S = \mathcal{O}(1)$. In the following, we shall see that when the gap size is smaller than the Debye length, i.e., $\beta < 1$, the physically relevant range 1.5 < ν < 3.5 contains an instability responsible for the spontaneous generation of a stable nonzero static electrical potential.

2.1.3. Mass Action Models. In this section, we discuss three distinct mass-action models, all of which lead to an effective decrease of the surface charge σ_d with increasing applied electrical potential. Following the notation,[29] we write first-order mass-action equations for equilibrated Z-covalent charged particles associated with adsorption/desorption in terms of Arrhenius-type coefficients. In the absence of electrical effects, the adsorption/desorption coefficients are denoted by k_a^{ne} and k_d^{ne}. In the presence of a dimensionless potential ϕ nondimensionalized by $k_B T/e$, these coefficients read

$$k_a = k_a^{ne}\, e^{-\lambda_a Z\phi} \quad k_d = k_d^{ne}\, e^{(1-\lambda_a)Z\phi} \tag{17}$$

where Z is the covalence and 0 < λ_a < 1 is an affinity factor describing the surface/ion interaction. As shown in refs 13,29, the equilibrium eq 17 leads to the Langmuir model with the normalized surface carrier concentration C_s given by the relation

$$C_s = \frac{1}{1 + \dfrac{k_d^{ne}}{k_a^{ne} C_b}\, e^{Z\phi}} \tag{18}$$

where C_b is the bulk ion concentration. Consequently, in the Langmuir model the normalized surface charge density $\sigma_d = ZC_s$ is a decaying function of the applied potential whenever $Z > 0$, as exemplified in Figure 2a.

Another popular mass-action kinetic model is the Frumkin−Fowler−Guggenheim (FFG) model, for which, in the absence of electrical potential, the adsorption/desorption coefficients display an Arrhenius-like dependence on the surface carrier concentration

$$k_a^{ne} = k_a^0\, e^{-\alpha(\Delta G/RT)C_s} \quad k_d^{ne} = k_d^0\, e^{(1-\alpha)(\Delta G/RT)C_s} \tag{19}$$

where ΔG is the standard net lateral interaction energy in the adsorbed layer and $\alpha\Delta G$ is the standard net activation energy due to lateral interactions, where 0 < α < 1. Using the relation eq 19 for equilibrated mass action leads to the following closed relationship between the applied electrical potential ϕ and the surface carrier concentration

$$Z\phi = \ln\left(\frac{1 - C_s}{\dfrac{k_d^0}{k_a^0 C_b} C_s\, e^{(\Delta G/RT)C_s}}\right) \tag{20}$$

This model also leads to a decreasing surface charge density as illustrated in Figure 2b.

Finally, the mass-action adsorption isotherm linearization in the specific case of cobalt-hexamine on silica surfaces proposed in ref 19 leads to the following surface charge-potential relation:

$$\sigma_d(\phi) = -n_{si} e \frac{1 - K_1 \exp(-3\phi)}{1 + K_2 \exp(-3\phi)} \tag{21}$$

where n_{si} = 0.5 nm^{-2} and $K_1 = 10^4$, $K_2 = 5 \times 10^3$. In this case, too, the surface charge density σ_d decreases monotonically with the applied surface potential (cf. Figure 2c). These mass-action models motivate our interest in the effect of the Stern boundary conditions eq 16 with $\nu > 0$.

2.2. Numerical Method. In the following, we restrict our study to steady states. In order to compute steady solutions of the above problem as a function of the experimentally easiest-to-change parameter β, we use a numerical continuation method (Auto-07p[30]) based on a Newton solver for the time-independent version of eqs 9−11 with the boundary conditions eq 12 and eq 16. To do so, the fields c, ρ, and ϕ are approximated by a high-order interpolant through the Gauss-Lobatto-Legendre points.[31] Equations 9−11 are discretized using a weak formulation, a procedure that enforces the corresponding boundary conditions eq 12 and eq 16. A similar treatment is applied to the linearized version of the equations and their derivative with respect to β.

Table 1. Summary of the Primary Eigenmodes[a]

trivial solution eigenmodes			
$\tilde{\phi} = 0, \tilde{c}, \tilde{\rho} = 0$		$\tilde{\phi}, \tilde{c} = 0, \tilde{\rho}$	
symmetric	antisymmetric	symmetric	antisymmetric
$\sigma = -(n+1)^2\pi^2$	$\sigma = -(2n+1)^2\pi^2/4$	$\sigma = -(n+1)^2\pi^2 - c\beta/2$	transcendental eq.
see eq 28	see eq 29	see eqs 30−31	see eqs 32−34

[a] The only eigenmodes that can lead to instability are those expressed by eqs 32−34.

3. LINEAR STABILITY ANALYSIS

3.1. The Trivial Solution and Its Stability. When the potential difference across the system vanishes, we may, without loss of generality, write $\phi_{\pm} = 0$. The problem in eqs 9−12 and eq 16 then has the trivial solution $(c, \rho) = (\bar{c}, 0)$ with $\phi = 0$. To analyze the stability of this solution, we linearize the equations and write the perturbation as $(\tilde{c}, \tilde{\rho}, \tilde{\phi})\exp(\sigma t)$, where σ is the temporal growth rate. This procedure leads to the eigenvalue problem

$$\Delta\tilde{c} = \sigma\tilde{c} \tag{22}$$

$$\Delta\tilde{\rho} + \bar{c}\Delta\tilde{\phi} = \sigma\tilde{\rho} \tag{23}$$

$$\Delta\tilde{\phi} = -\frac{\beta}{2}\tilde{\rho} \tag{24}$$

The corresponding linearized boundary conditions are

$$\partial_x\tilde{c} = \partial_x\tilde{\rho} + \bar{c}\partial_x\tilde{\phi} = 0 \quad \text{at} \quad x = \pm 1 \tag{25}$$

$$\partial_x\tilde{\phi} \mp \nu\sqrt{\beta}\tilde{\phi} = 0 \quad \text{at} \quad x = \pm 1 \tag{26}$$

The integral constraints on the perturbation become

$$\langle\tilde{c}\rangle = \langle\tilde{\rho}\rangle = 0 \tag{27}$$

Because the equation for $\tilde{c}$ decouples, the form of an eigenmode $(\tilde{c}, \tilde{\rho})$ is either $(\tilde{c}, 0)$ with $\tilde{\phi} \equiv 0$ or $(0, \tilde{\rho})$ with $\tilde{\phi} \neq 0$. Solving equation eq 22 with the first boundary condition in eq 25 and the first constraint in eq 27, we find that $\tilde{c}$ is either symmetric, $\tilde{c} \equiv \tilde{c}_s$ with $\tilde{c}_s(x) = \tilde{c}_s(-x)$, or antisymmetric, $\tilde{c} \equiv \tilde{c}_a$ with $\tilde{c}_a(x) = -\tilde{c}_a(-x)$

$$\tilde{c}_s = \cosh(\sqrt{\sigma}x) \quad \text{with} \quad \sigma = -(n+1)^2\pi^2 \tag{28}$$

$$\tilde{c}_a = \sinh(\sqrt{\sigma}x) \quad \text{with} \quad \sigma = -(2n+1)^2\frac{\pi^2}{4} \tag{29}$$

where $n = 0, 1, \cdots$ is a non-negative integer. Likewise, when $\tilde{c} = 0$, we set $\lambda^2 \equiv \sigma + [\bar{c}\beta/2]$ and find that $\tilde{\rho}$ is either symmetric, $\tilde{\rho} \equiv \tilde{\rho}_s$

$$\tilde{\rho}_s = \cosh(\lambda x) \quad \text{with} \quad \sigma = -(n+1)^2\pi^2 - \frac{\bar{c}\beta}{2} \tag{30}$$

with associated potential

$$\tilde{\phi}_s = -\frac{\beta}{2\lambda^2}\cosh(\lambda x) + \frac{\beta}{2\lambda^2}(-1)^{n+1} \tag{31}$$

or antisymmetric, $\tilde{\rho} \equiv \tilde{\rho}_a$

$$\tilde{\rho}_a = \sinh(\lambda x) \tag{32}$$

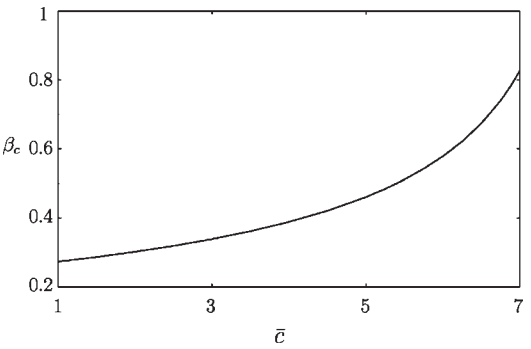

Figure 3. Evolution of the location of the primary bifurcation β_c as a function of the mean concentration $\bar{c}$ as computed from eq 35 for $\nu = 2$.

with associated potential

$$\tilde{\phi}_a = -\frac{\beta}{2\lambda^2}\sinh(\lambda x) + \frac{1}{\bar{c}}\left(\frac{\beta\bar{c}}{2\lambda} - \lambda\right)x\cosh\lambda \tag{33}$$

Imposition of the boundary conditions eq 25 leads to a transcendental equation for the associated eigenvalue σ

$$1 - \nu\sqrt{\beta} = \frac{\bar{c}\nu\beta^{3/2}}{2\lambda^2}\left(\frac{1}{\lambda}\tanh\lambda - 1\right) \tag{34}$$

A summary of the eigenmodes of the trivial solution is given in Table 1. These results indicate that the only eigenmodes that can be unstable ($\sigma > 0$) are of the form $(0, \tilde{\rho}_a)$. From eq 34, we first observe that, for $\nu > 0$, a singularity appears at $\beta = \beta_s \equiv 1/\nu^2$. At this value, $\sigma \to \infty$ and the potential $\tilde{\phi}_a$ diverges at all $x \in [-1, 1]$ except $x = 0$ (see eq 33). To locate bifurcations, we set $\sigma = 0$ in eq 34. This provides a criterion for stability: if $\nu \leq (\bar{c}/2)^{1/2}$, no instability from the trivial solution can occur. If, on the other hand, $\nu \geq (\bar{c}/2)^{1/2}$ there is a critical dimensionless gap β_c at which the trivial state changes stability given by

$$\beta_c = \frac{1}{2\bar{c}}\left(\ln\frac{\nu + \sqrt{\bar{c}/2}}{\nu - \sqrt{\bar{c}/2}}\right)^2 \tag{35}$$

The dependence of β_c on $\bar{c}$ is shown in Figure 3. A more detailed analysis of eq 34 reveals that this is the only bifurcation of the trivial state and hence that any bifurcation from the trivial state must correspond to an antisymmetric eigenmode. The structure of the unstable eigenmode is shown in Figure 4 for $\bar{c} = 2$, $\nu = 2$, and $\beta = 0.3 < \beta_c \equiv 0.3017$. Moreover, eq 34 shows that σ decreases to $-\infty$ as β approaches $\beta_s = 0.25$ from below and increases to $+\infty$ when β approaches β_s from above. Thus, when $\beta > \beta_c > \beta_s$ (respectively, $\beta_c > \beta > \beta_s$), the trivial state is stable (respectively unstable).

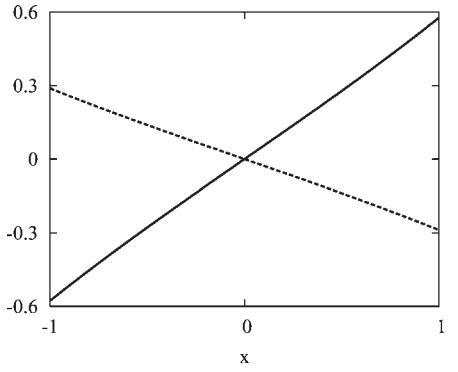

Figure 4. The marginal antisymmetric eigenmode $(\tilde{\rho}, \tilde{\phi})$ versus x for $\bar{c} = 2$, $\beta = 0.3017$, $\nu = 2$. The solid line denotes the charge density perturbation $\tilde{\rho}_a$ in eq 32 and the broken line the electrical potential perturbation $\tilde{\phi}_a$ in eq 33.

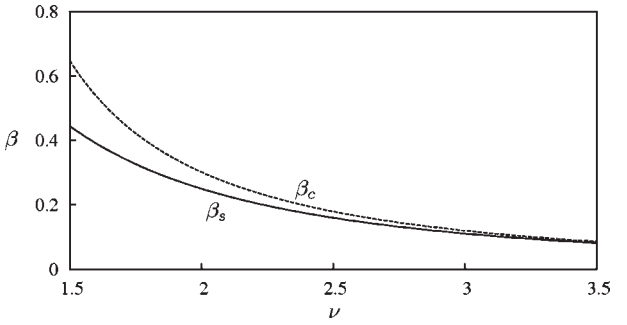

Figure 5. Location β_s of the singularity and β_c of the bifurcation point as a function of the aspect ratio of the boundary layer ν when $\bar{c} = 2$. Both locations approach $\beta = 0$ monotonically as $\nu \to \infty$, with $\beta_s < \beta_c$.

The variation of β_s and β_c with the aspect ratio ν of the boundary layer is illustrated in Figure 5 for $1.5 < \nu < 3.5$. When ν increases, i.e., when the Stern layer becomes smaller and smaller compared to the Debye layer, β_c decreases toward β_s and the interval of instability decreases. Asymptotically, the case $\nu \gg 1$ corresponds to a constant imposed potential—Dirichlet boundary conditions for the Poisson−Boltzmann problem eq 9—at the solid boundary and in this system there is no bifurcation of the trivial state.

3.2. Analysis of the Growth Rate Divergence near β_s. Let us now turn to the divergence of the growth rate near $\beta_s \equiv 1/\nu^2$. We write

$$\beta = (1 + \varepsilon)/\nu^2 \tag{36}$$

where $|\varepsilon| \ll 1$ measures the distance to the singularity, and obtain from eq 34 the following leading order balance

$$\sigma \sim \frac{\bar{c}}{\nu^2 \varepsilon} \sim \frac{\bar{c}}{\nu^2(\nu^2\beta - 1)} \tag{37}$$

valid when $|\varepsilon| \ll 1$. A comparison between this relation and the numerical results presented in Figure 6 confirms the validity of this leading order asymptotic behavior.

4. NONLINEAR REGIME

We now turn to the study of the nontrivial solutions created at $\beta = \beta_c$, and consider the case with no electric field imposed across the layer separately from the case with an imposed electric field.

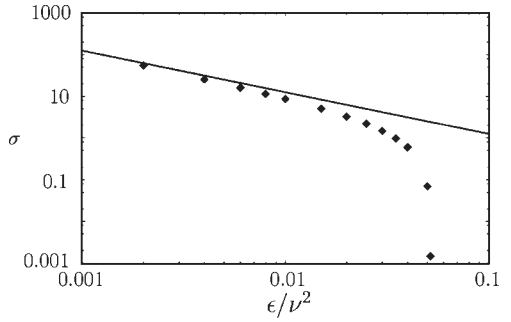

Figure 6. Asymptotic behavior of the eigenvalue σ as a function of ε/ν^2, i.e., $\beta - \beta_s$ when $\bar{c} = 2$, $\nu = 2$. The solid line represents the analytical prediction eq 37, while the squares are numerical results obtained with 81 mesh points.

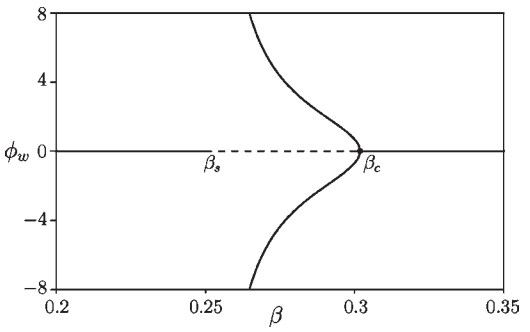

Figure 7. This bifurcation diagram shows the dependence of the electrical potential ϕ_w at the right wall on β in the case of a closed system with no imposed electric field and $\bar{c} = 2$, $\nu = 2$. Resolution uses 41 mesh points. Solid (respectively dashed) lines refer to stable (respectively unstable) solutions. The trivial solution loses stability at $\beta_s = 0.25$ before recovering it after a supercritical pitchfork bifurcation at $\beta_c = 0.3017$. This pitchfork creates two stable nonlinear branches of antisymmetric states whose amplitude diverges near β_s.

The bifurcation diagrams exhibited below show ϕ_w, the potential at the right wall, as a function of the parameter β. As shown by Plouraboué and Chang,[9] this potential is directly linked to the amplitude of the interaction between the walls. This relation is modified here by the constraint eq 13 imposing global charge neutrality but the results for different choices of $\bar{c}$ are qualitatively similar.

4.1. Nontrivial Solutions with No Imposed Electric Field. *4.1.1. Numerical Results.* As already mentioned, in the absence of an imposed electric field we may set $\phi_+ = \phi_- = 0$. The resulting problem has the solution $(c, \rho) = (\bar{c}, 0)$ with $\phi = 0$, valid for any value of β. We refer to this solution as the trivial state and study the solutions resulting from the instability of this state at $\beta = \beta_c$.

Equations 9−11 with the boundary conditions eq 12 and eq 16 are invariant under two symmetry operations, the operation S:$(c, \rho, \phi) \to (c, -\rho, -\phi)$, $x \to x$, and the spatial reflection S_Δ:$(c, \rho, \phi) \to (c, \rho, \phi)$, $x \to -x$.

The type of bifurcation that takes place at $\beta = \beta_c$ depends on the symmetry properties of the marginally stable eigenfunction. We showed that, at $\beta = \beta_c$, the marginal eigenmode takes the form $(\bar{c}, \tilde{\rho}, \tilde{\phi}) = (0, \tilde{\rho}_a, \tilde{\phi}_a)$ with $\tilde{\rho}_a(x) = -\tilde{\rho}_a(-x)$, $\tilde{\phi}_a(x) = -\tilde{\phi}_a(-x)$. This eigenvector breaks both the S and S_Δ symmetries but is invariant under $S \circ S_\Delta = S_\Delta \circ S$. We expect therefore that the

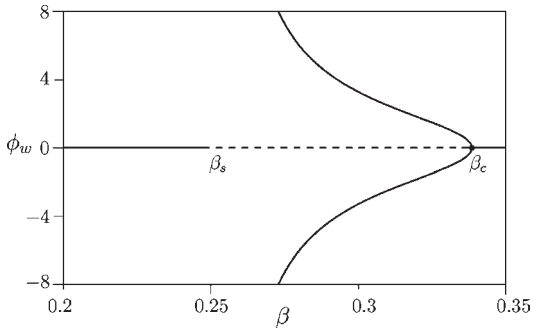

Figure 8. As for Figure 7 but with $\bar{c}$ = 3, yielding β_c = 0.3386. The resolution uses 41 mesh points.

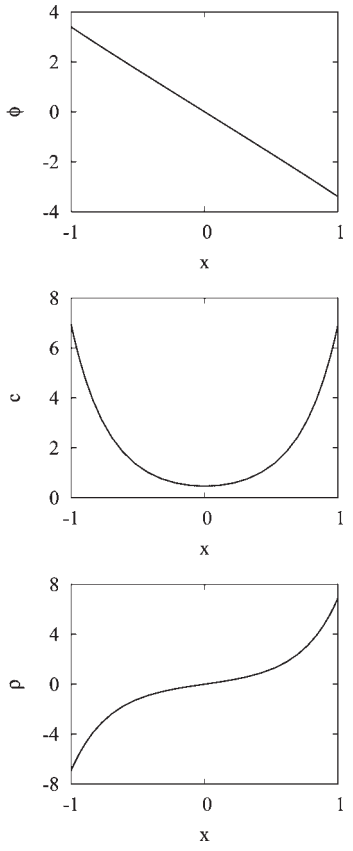

Figure 9. Nonlinear solutions on the lower solution branch in Figure 7 for $\bar{c}$ = 2, ν = 2, and β = 0.28 using 41 mesh points. Note that c is symmetric and nonzero.

bifurcation at β_c is a pitchfork. Figure 7 and Figure 8 show the resulting bifurcation diagrams for ν = 2 and $\bar{c}$ = 2, $\bar{c}$ = 3, respectively. Solid (broken) lines correspond to linearly stable (unstable) solutions. The trivial state corresponds to $\phi_w = 0$. As predicted by linear theory, this state is unstable for $\beta_s = 0.25 < \beta < \beta_c$ = 0.3017 ($\bar{c}$ = 2), 0.3386 ($\bar{c}$ = 3). At $\beta = \beta_c$, the branch undergoes a *supercritical* pitchfork bifurcation as β *decreases*, producing two branches. Solutions along each branch are related by the broken symmetry (S or S_Δ that in the present case produce the same solution) and are therefore dynamically equivalent. Both inherit the stability properties of the bifurcating trivial solution and are therefore *stable*. Sample solutions are shown in Figure 9 for $\bar{c}$ = 2, ν = 2 and β = 0.28. With further decrease in β

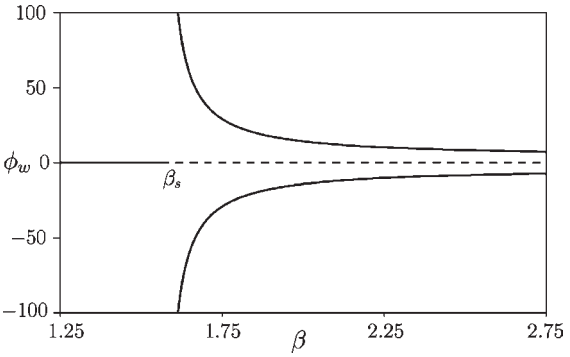

Figure 10. This bifurcation diagram shows the dependence of the electrical potential ϕ_w at the right wall on β in the case of a closed system with no imposed electric field and $\bar{c}$ = 2, ν = 0.8. Resolution uses 29 mesh points. Solid (respectively dashed) lines refer to stable (respectively unstable) solutions. The trivial solution loses stability at β_s = 1.5625.

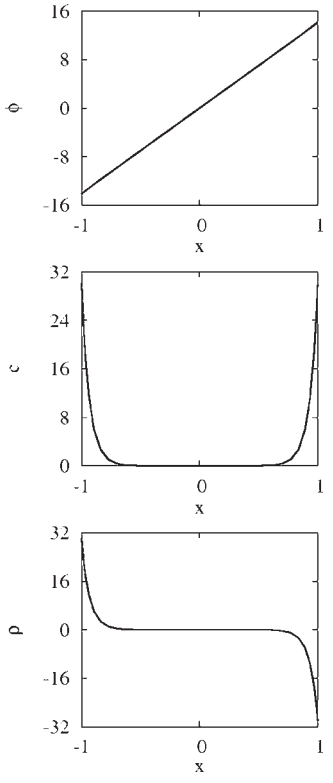

Figure 11. Nonlinear solutions on the upper solution branch in Figure 10 for $\bar{c}$ = 2, ν = 0.8, and β = 2 and 41 mesh points. The electrical potential is nearly linear with the double layer structure clearly visible in the concentration and charge density profiles.

both branches diverge, at $\beta = \beta_s$, independently of the value of $\bar{c}$. In fact, a divergence is present at this parameter value in the steady state potential $\phi(x)$ at all locations $|x| \leq 1$ in the domain except $x = 0$.

Figure 10 shows the bifurcation diagram for $\bar{c}$ = 2 and ν = 0.8. The nonlinear solution branches persist and remain stable throughout. Both branches continue to diverge at β_s but no longer bifurcate from the trivial state which remains unstable for all values of $\beta > \beta_s$. However, since β_s is now larger the electrical double layer in the corresponding solutions is sharper (Figure 11).

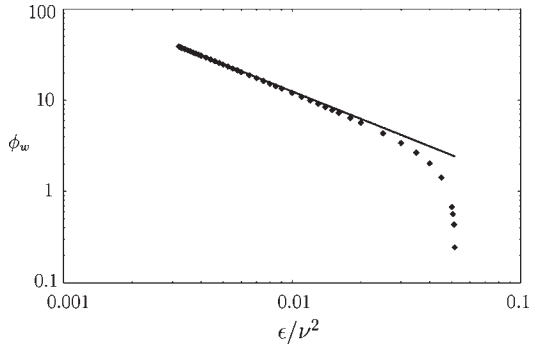

Figure 12. Asymptotic behavior of the electrical potential ϕ_w at the right wall as a function of ε/ν^2, i.e., $\beta - \beta_s$ when $\bar{c} = 2$, $\nu = 2$. The solid line represents the analytical prediction eq 55 while the squares are numerical results obtained with 81 mesh points.

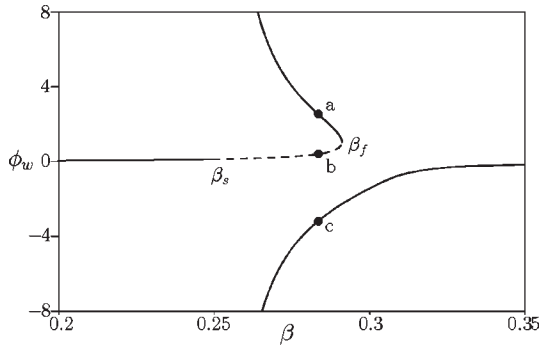

Figure 13. This bifurcation diagram shows the dependence of the electrical potential ϕ_w at the right wall on β in the case of a closed system with an imposed electric field ($\phi_0 = 0.01$) and $\nu = 2$. Resolution uses 41 mesh points. The applied potential difference is 2% of the thermal potential. Solid (respectively dashed) lines refer to stable (respectively unstable) solutions. The imperfect pitchfork bifurcation produces a fold, here observed at $\beta_f = 0.2911$. The upper branch loses stability at $\beta_s = 0.25$ and recovers it after the fold. The lower branch is always stable. Both branches diverge at β_s. Points *a*, *b*, and *c* correspond to the solutions shown in Figure 14.

4.1.2. Analysis of the Divergence of the Stationary Solution near β_s. The singular behavior of the nonlinear solutions at β_s is, like the growth rate divergence in the linear problem, a consequence of the global charge constraint eq 13. To analyze the origin of this behavior, we adopt the parametrization eq 36 in the vicinity of β_s and restrict attention to the branch of nonlinear solutions with $\phi_w > 0$. After integrating once the stationary solutions of eqs 10−11 with the boundary conditions eq 12 and eq 16, it is possible to obtain a general expression for the total concentration and density

$$c = 2e^{\gamma}\cosh(\phi + \delta) \tag{38}$$

$$\rho = -2e^{\gamma}\sinh(\phi + \delta) \tag{39}$$

where γ and δ are two constants of integration. The normalization conditions eq 13 imply that $\delta = 0$ and yield an integral condition determining the second constant of integration γ

$$e^{\gamma} = \frac{\bar{c}}{\int_{-1}^{1}\cosh\phi\,dx} \tag{40}$$

The constant γ can be found from an implicit integral relation that we now establish.

The governing equation eq 9 with ρ from eq 38 has the first integral

$$\frac{1}{2}(\partial_x\phi)^2 = \beta e^{\gamma}(\cosh\phi + d) \tag{41}$$

where d is a further constant of integration. Integrating once more and making use of the relation eq 40, we obtain

$$\frac{1}{2}\int_{-1}^{1}(\partial_x\phi)^2\,dx = \beta(\bar{c} + 2de^{\gamma}) \tag{42}$$

The constant d is determined by the boundary conditions eq 16 and eq 41

$$d = \frac{1}{2}\nu^2{\phi_w}^2 e^{-\gamma} - \cosh\phi_w \tag{43}$$

where ϕ_w is the potential at the wall, $\phi_w = \phi(1)$. We now rewrite the left-hand side of eq 42 using the parity of the integrand

$$\frac{1}{2}\int_{-1}^{1}(\partial_x\phi)^2\,dx = \int_{0}^{\phi_w}\partial_x\phi\,d\phi \tag{44}$$

and combine eqs 41−44 to obtain

$$\sqrt{de^{\gamma}}\int_{0}^{\phi_w}\sqrt{1 + \frac{\cosh\phi}{d}}\,d\phi = \sqrt{\frac{\beta}{2}}(\bar{c} + 2de^{\gamma}) \tag{45}$$

Equations 43 and 45 provide a transcendental equation for the constant γ. This equation requires the knowledge of the potential ϕ in order to compute the integral on the left, as well as the wall potential ϕ_w.

It is necessary therefore to solve for the potential ϕ near the singularity. Since the wall potential diverges at the singularity, so does $\cosh\phi$. Hence, the integral $\int_{-1}^{1}\cosh\phi\,dx$ in eq 40 will also diverge and we may anticipate that the constant γ approaches $-\infty$ monotonically as a function of the departure ε from the singularity. Consequently, we set $e^{\gamma} \equiv \bar{\varepsilon}$, where $\bar{\varepsilon}$ is a small parameter with monotone dependence on ε. This setup provides the relevant asymptotic ordering required to find the dependence of $\bar{\varepsilon}$ on ε and thereby to identify the singularity in the wall potential when the dimensionless gap β approaches β_s. To do so, we insert the above Ansatz in the governing equation for the potential

$$\Delta\phi = \beta e^{\gamma}\sinh\phi = \beta\bar{\varepsilon}\sinh\phi \tag{46}$$

The small forcing term on the right-hand side suggests the following expansion for the potential near β_s:

$$\phi = \phi^0 + \bar{\varepsilon}\phi^1 + O(\bar{\varepsilon}^2) \tag{47}$$

At leading order, the homogeneous problem

$$\partial_{xx}^2\,\phi^0 = 0 \tag{48}$$

$$\partial_x\phi^0|_{x=\pm 1} = \pm\nu\sqrt{\beta}\phi^0 \tag{49}$$

leads to the simple linear solution

$$\phi^0(x) = \nu\sqrt{\beta}\phi_w x \tag{50}$$

Close to the singularity, $\nu(\beta)^{1/2} \to 1$ so that the integral in eq 40 required to compute the constant γ yields

$$e^{\gamma} \simeq \bar{c}\phi_w e^{-\phi_w} \tag{51}$$

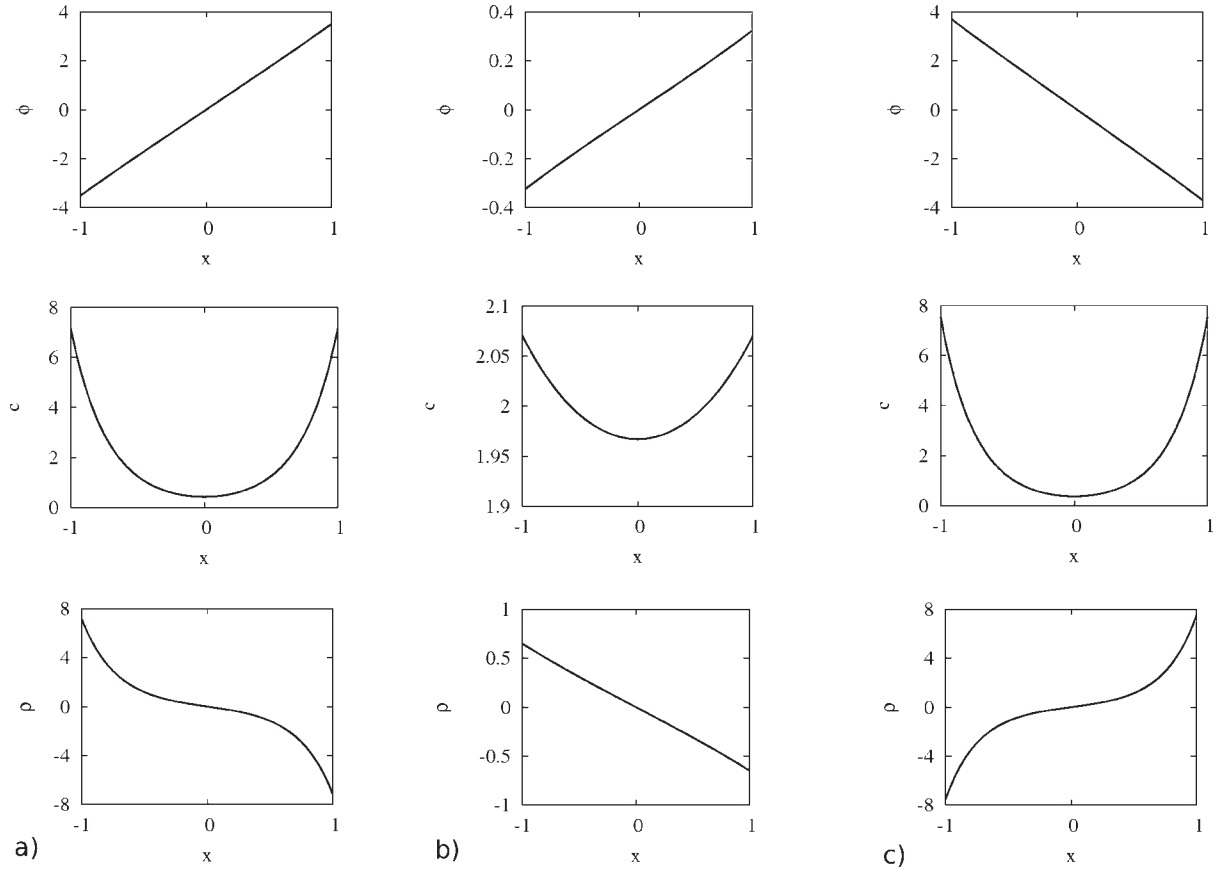

Figure 14. Solutions in 4.2 for $\bar{c} = 2$, $\nu = 2$, $\phi_0 = 0.01$, and $\beta = 0.28$ at the locations indicated, obtained with 41 mesh points. (a) left column: solution from the upper branch, (b) middle column: solution from the middle branch, (c) right column: solution from the lower branch.

Using eq 51 in the definition eq 43, we see that, near β_s, $d \gg \cosh \phi_w \geq \cosh \phi(x)$. Since $\cosh \phi/d \ll 1$, we expand the integrand on the left-hand side of eq 45, and by integrating only the leading order term, we obtain

$$\sqrt{de^{\gamma}}\phi_w \simeq \sqrt{\frac{\beta}{2}}(\bar{c} + 2de^{\gamma}) \tag{52}$$

We next approximate the quantity $(de^{\gamma})^{1/2}$ on the left-hand side of eq 52 using eq 51

$$\sqrt{de^{\gamma}} \simeq \frac{\nu\phi_w}{\sqrt{2}}\left(1 - \frac{\bar{c}}{2\nu^2\phi_w}\right) \tag{53}$$

Inserting the approximation eq 53 into eq 52 and using the scaling eq 36 for β, we obtain finally the following balance between the wall potential ϕ_w and the distance ε to the singular dimensionless wall gap β_s

$$\frac{\nu\phi_w{}^2}{\sqrt{2}}\left(1 - \frac{\bar{c}}{2\nu^2\phi_w}\right) = \frac{1}{\sqrt{2}\nu}\left(1 + \frac{\varepsilon}{2}\right)(\bar{c} + \nu^2\phi_w^2 - \bar{c}\phi_w) \tag{54}$$

This expression leads to an explicit relation between the wall potential, the constant γ, the previously introduced small parameter $\bar{\varepsilon}$ and the distance from singular behavior as measured by ε

$$\phi_w \simeq \frac{\bar{c}}{\nu^2\varepsilon} \sim \frac{\bar{c}}{\nu^2(\nu^2\beta - 1)} \tag{55}$$

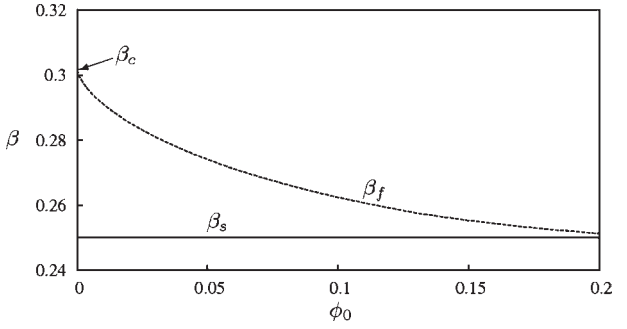

Figure 15. The locations of the singularity β_s and of the fold β_f as a function of ϕ_0 when $\bar{c} = 2$, $\nu = 2$. The imposed electrical field has no influence on the location of the singularity, but unfolds the pitchfork bifurcation at β_c thereby creating a fold at β_f (see Figure 13).

$$\bar{\varepsilon} = e^{\gamma} \simeq \frac{\bar{c}^2}{\nu^2\varepsilon} e^{-\bar{c}/\nu^2\varepsilon} \tag{56}$$

A comparison between this analytical result and the numerical results is shown in Figure 12. The numerical results agree well with the analytical prediction.

4.2. Imposed Electric Field. We next consider the case where $\phi_+ \neq \phi_-$ corresponding to an imposed electric field, as considered by Bazant et al.[8] Since a constant can be added to the

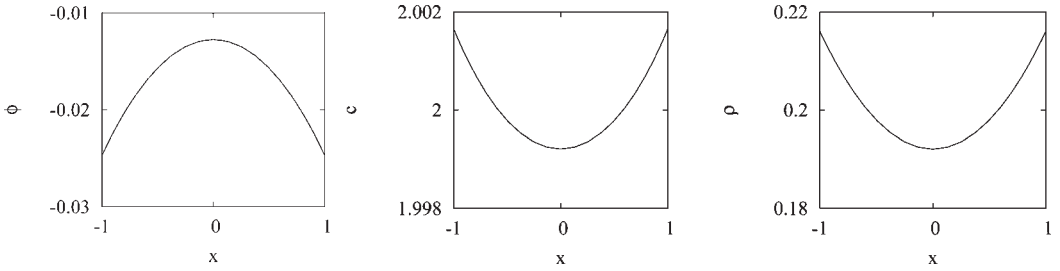

Figure 16. Plots of the stable potential, concentration, and density profiles for a nonelectroneutral electrolyte with $\overline{\rho} = 0.2$ and $\bar{c} = 2$ computed for dimensionless half-gap $\beta = 0.245$, just below the singularity at $\beta_s = 1/\nu^2 = 0.25$.

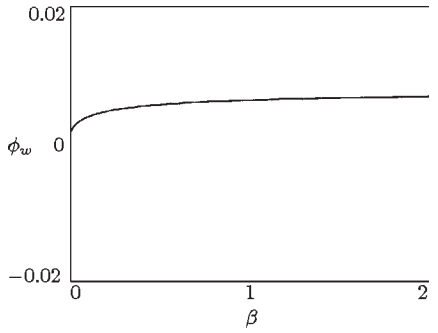

Figure 17. Bifurcation diagram showing the stable trivial solution in the case $\nu = -2$ and an applied potential difference equal to 2% of the thermal potential. The remaining parameters are as in Figures 7, 8, and 13.

values of ϕ_+ and ϕ_- without changing the solution (c, ρ), we study the general case in which the boundary condition on ϕ is rewritten as $\partial_x\phi = \pm\nu\,\beta^{1/2}(\phi \mp \phi_0)$ at $x = \pm 1$, where $\phi_0 \neq 0$, so that $\phi_+ = -\phi_- = \phi_0$ providing an electrically neutral system. We take $\phi_0 = 0.01$, representing a potential difference of 2% of the thermal potential k_BT.

The main effect produced by the imposed electric field is the destruction of the trivial equilibrium state $(c, \rho) = (\bar{c}, 0)$. Equations 9−11 with the boundary conditions eq 12 and eq 16 no longer have any symmetry. As a consequence, we expect that the primary bifurcation becomes imperfect when ϕ_0 is small but nonzero. Figure 13 shows the resulting bifurcation diagram and confirms this expectation. The lower branch, $\phi_w < 0$, $\beta > \beta_s$, is always stable, while the upper branch, $\phi_w > 0$, loses stability with increasing β at β_s and then passes through a fold at β_f and recovers stability. Note that $\beta_s \leq \beta_f \leq \beta_c$. Different steady solutions corresponding to the same value of β are shown in Figure 14. The dependence of β_f and β_s on the potential difference ϕ_0 is shown in Figure 15; the imposed electric field does not affect the value at which the nontrivial solutions diverge. Additionally, reversing the sign of the imposed electric field changes the bifurcation diagram in a simple way: the fold now appears on the lower branch and is absent from the upper branch.

4.3. Doubly Diffusive Effects. It is important, finally, to mention that we can also analyze the possible influence of double diffusion on the electrolyte dynamics. Let us first note that double diffusion results in different time scales for charge density and charge concentration dynamics. Indeed, on inspecting the Nernst−Planck equations (eq 3) one sees that each diffusion coefficient can be factored from the right-hand side because both the electroconvective and the diffusive fluxes are proportional to it. On adding and subtracting the anionic and cationic concentrations to obtain the dynamical equations associated with the charge density and total concentration, one finds that different time scales are present in each equations. These time scales obviously impact the transient states such as those studied by Bazant et al.[8] However, they do not change the steady states, and do not change the stability of the trivial solution. Moreover, although additional secondary bifurcations are in general possible, our results show that double diffusion does not qualitatively impact the results already obtained, although it does affect the instability growth rates. In particular, no Hopf bifurcations leading to oscillatory dynamics of the charge distribution were located while changing the diffusivity ratio between 0.1 and 10, even when applying a supplementary potential difference.

4.4. The Nonneutral Case $\overline{\rho} \neq 0$. We next turn to the case of an electrolyte with nonzero global charge density, a case studied experimentally at the nonelectroneutral point pH $\neq 7$ in ref 32. The resulting solution profiles, displayed in Figure 16, differ quantitatively from the electroneutral case, since the profiles of the potential, concentration, and charge density are now all parabolic. In the case of the potential, this profile is the result of symmetric forcing associated with the Coulomb source terms. Despite these differences, we find that the system behaves exactly as in the electroneutral case $(\phi = 0, c = 2, \overline{\rho} = 0)$. In particular, all the main features of the bifurcation diagram are recovered, including the presence of the singularity at $\beta = \beta_s$ that is simultaneously responsible for the change in stability of the trivial state and the divergence of the nonsymmetric solution that bifurcates from the trivial state at $\beta_c > \beta_s$, cf. Figure 7. A detailed numerical study of the divergent behavior of the solution in the vicinity of the singularity $\beta = \beta_s$ follows the analytical properties identified in relations eqs 55−56. Indeed, the asymptotic analysis developed in section 4.1.2 can be easily extended to the nonelectroneutral case, with the important difference that the constant $\delta \equiv \tanh^{-1}(\overline{\rho}/\bar{c})$ in relations eqs 38−39 now differs from zero. The wall potential ϕ_w again diverges at β_s following the prediction eq 55, and the potential variation for $\beta > \beta_s$ follows the asymptotically linear trend found in eq 50 and confirmed in Figure 11.

4.5. The Case $\nu < 0$ in the Stern Layer Boundary Condition. Let us also comment on the choice $\nu < 0$ in the Stern layer boundary condition, as considered in refs 8 and 27. In this case, the stability result is dramatically different. There are no solutions apart from the trivial solution which remains stable for all values of β. In the absence of an applied electric field, the stability analysis for the trivial state in section 3 and the corresponding relations (eqs 34−35) do not generate either bifurcation or singularity. This theoretical observation complements the analysis of the bifurcation diagram in the presence of an applied electric field as exemplified in Figure 17.

5. DISCUSSION AND CONCLUSION

5.1. Discussion. *5.1.1. Instability Mechanism.* In this paper, we have analyzed the properties of electro-osmotic flows confined between parallel plates, focusing on gap widths $2h$ on the order of the Debye length λ_D. We have shown that, in the presence of Stern layers, there is a range of gaps for which an electroneutral but charged electrolyte is unstable and a stable potential difference is spontaneously generated despite thermodynamic equilibrium.

To understand the physical origins of the instability of the trivial state when $\nu > 0$, we recall (see section 3) that the perturbation in the total concentration decouples from the perturbations of both the charge density and the potential. Thus, all concentration perturbations decay, as described by eq 28 and eq 29, and instability arises from the coupling between charge density fluctuations and the potential. This coupling leads to eqs 22−23, and hence to an eigenvalue problem of Poisson type

$$\Delta\tilde{\rho} - \beta\tilde{\rho} = \sigma\tilde{\rho} \tag{57}$$

where $\tilde{\rho}$ is the density perturbation and σ is the eigenvalue. The first term of the left side of eq 57 describes diffusion of the perturbation and is stabilizing. The second term on the left arises from electroconvection. Since $\beta > 0$, this term is also stabilizing. Hence, one has to look to the boundary conditions for the source of instability. Equations 25 and 26 show that the perturbation of the potential in the Stern layer generates a nonzero charge flux, $\partial_x\overline{\rho} = \mp\overline{c}\nu\sqrt{\beta}\tilde{\phi}$ at $x = \pm 1$. Thus, when $\nu > 0$ an increase in the potential $\tilde{\phi}$ on the wall (and hence an increase in the positive charge) leads to an increased flux of (positive) charge to the wall. This positive feedback is in turn responsible for the instability, and the instability is thus a consequence of the charge regulation process. The strength of the feedback mechanism scales with $\sqrt{\beta}$ and so increases with increasing β. However, for large gaps, $\beta \gg 1$, the destabilizing mechanism is suppressed by the stabilizing electroconvection effect which is proportional to β. Likewise, for very small gaps, $\beta \ll 1$, the destabilizing term is dominated by the stabilizing effect of diffusion. Thus, straightforward balances between the different physical effects explain qualitatively the range of values of the parameter β for which instability occurs. The detailed calculations in section 3 confirm this basic picture. Note that no instability is predicted for $\nu < 0$ and none is found.

The parameter range for which this occurs is most easily given in terms of the parameter $\beta \equiv h^2/\lambda_D^2$: $\beta_s \equiv 1/\nu^2 < \beta < \beta_c \equiv 1/2\overline{c}\{\ln[(\nu + (\overline{c}/2)^{1/2}]/[\nu - (\overline{c}/2)^{1/2}]\}^2$, where $\nu \equiv \lambda_D/\lambda_S$ is the ratio between the Debye length and the width of the Stern layer. Figure 5 shows the range of values of β (between the continuous and dotted lines) for which this is the case. For large Debye lengths, the range is narrow but broadens considerably as the Debye length approaches the Stern length. This regime is both of physical interest and relevant to experimental observations;[9] consequently, the generation of a spontaneous potential difference across the gap should be accessible to experimental confirmation. For a confined system ($\overline{c} = 2$), the typical values of the Stern length $\lambda_S = 5$ nm and the Debye length $\lambda_D = 10$ nm indicate that $\nu = 2$ and hence that the instability sets in at $\beta = 0.3017$, i.e., at a wall gap $2h \simeq 11$ nm. This property of the system is a consequence of the overlap of the double layers resulting in nonlinear interactions that lead to a preferred antisymmetric potential difference. Indeed, when the overlap zone is sufficiently large, both double layers compete and destabilize the trivial solution. As a result, any small perturbation grows and evolves into an antisymmetric solution.

The instability threshold β_c diverges when $\nu \to (\overline{c}/2)^{1/2}$, and for $0 < \nu < (\overline{c}/2)^{1/2}$ the trivial solution is stable. For the confined system of interest, $\overline{c} = 2$. Since the Stern length associated with the width of the ion adsorption layer is always smaller than the Debye length, this regime of stability is not accessible in physical systems. In contrast, when $\nu > (\overline{c}/2)^{1/2}$ the trivial solution is stable at large β but loses stability at the critical value $\beta = \beta_c$ as β decreases. This value is on the order of 1 implying that stability is lost when the gap is on the order of the Debye length. A nontrivial antisymmetric steady solution emerges from the trivial branch through a supercritical bifurcation, i.e., in the direction of decreasing β. When the gap width is twice the Stern length, the nontrivial branch diverges to infinity and, at the same time, the neutral solution restabilizes.

5.1.2. Divergent Behavior of the Potential. In section 4.1.2, we showed that there is a critical gap for which the stable attractive solution diverges, leading to large and potentially infinite surface potential and charge. The analytical study of this behavior in the vicinity of this singularity is consistent with our numerical results, confirming that the presence of the singularity is a property of the mathematical model, and in particular a consequence of the imposition of overall charge balance—whether electroneutral or not.

The singularity results from a "reduced" charge regulation effect at the solid surface combined with Poisson−Boltzmann nonlinearities. These imply that increasing the charge on one surface increases the potential on the other, with increasing but opposite charges on the two surfaces owing to the overall charge conservation constraint. For antisymmetric solutions, this constraint thus leads to an increase in the potential difference between the surfaces. This effect increases with decreasing gap width and is in turn enhanced by growing nonlinear terms. Furthermore, the singular behavior appears precisely when the Stern layers of the two surfaces first touch (Figure 1c) implying that no electrical breakdown occurs unless the Stern layers overlap. This is physically reasonable, since ion adsorption precludes gap widths equal to or greater than typical electron cloud separations. Hence, even if the singularity is an artifact of the model, it is physically clear that bringing two solids closer together than a Stern length will involve strong repulsive forces associated with short-range hard-sphere repulsion. Therefore, the singularity identified here also represents a limit on the possible distance between the two solid surfaces. With the same physical parameters used previously ($\lambda_S = 5$ nm, $\lambda_D = 10$ nm, and $\nu = 2$), this distance is $2h = 10$ nm.

It is important, however, to stress that the singularity is unphysical, since very high values of the electrical potential are inconsistent with the dilute Poisson−Boltzmann approximation.[33] At very high potentials, other mechanisms such as limiting current or Faradaic electron transfer reactions[34] become important, but these have not been included in the model studied here. Furthermore, at very small distances other forces such as strong repulsive van der Waals/Lennard-Jones potentials will overcome the attractive Coulomb forces considered in this study, smoothing out the associated singularity. Nevertheless, the prediction of a strong attractive interaction at small distances could provide an explanation for the observation of just such interactions.[20,21] Moreover, since the singularity is also associated with a divergence of the total electrical energy, our findings are also likely relevant to the design and use of electrolyte solutions in

nanometer-sized sheets for electrical storage.[35−37] The high surface potential dependence with a reduced charge regulation effect in Stern layers emphasizes the tremendous role of adsorption kinetics in confined systems, and provides a rationale for the choice of chemically relevant systems in highly compact double-layer-scale capacitors. Our results predict an explicit dimensionless gap range (between β_s and β_c) for which these desirable surface potentials arise, and its dependence on the parameters characterizing the adsorption kinetics of the chosen materials.

5.1.3. Bifurcation Diagrams. Let us now comment on the generality of our results. It is an important observation that the bifurcation diagrams associated with the different solutions we have identified here appear to be a generic property of this type of physical system, since similar diagrams characterize both different parameter values and different variants of the same system. For example, we have changed the ratio ν between the Debye and Stern lengths widely without finding any new solution branches. Adding an imposed electric field modifies the trivial state and unfolds the supercritical pitchfork bifurcation in the field-free case, replacing it by a fold bifurcation, at a new threshold value β_f, in an entirely predictable manner. This local change in behavior does not alter our main conclusion that for small gaps there is a range of parameter values in which nontrivial steady antisymmetric solutions are stable. These conclusions remain qualitatively unchanged when different anion and cation diffusivities are included or when nonelectroneutrality is permitted. Thus, the conclusions of our study are robust, and no new effects arise when the model assumptions are relaxed.

5.2. Conclusion. The analysis of electrokinetic dynamics at nanometer scales opens new directions for research on electroosmosis. In this paper, we followed the classical mean-field Poisson−Boltzmann−Nernst−Planck description associated with double-layer electrokinetics. We have considered the simplest model, consisting of an infinite slot configuration and one-dimensional field variations perpendicular to the parallel solid surfaces, but have taken into account the overlap of double layers and the influence of the associated Stern layers. At a distance on the order of the Debye length, a nontrivial antisymmetric steady-state solution bifurcates supercritically from the trivial electroneutral state through a pitchfork bifurcation. This solution is stable between this length scale and the shorter Stern length. At separations resulting in overlap of the Stern layers, a second transition takes place, where the stable nontrivial solution diverges. These properties persist within more elaborate models and are therefore likely to be of interest in future work.

■ AUTHOR INFORMATION

Corresponding Author

*E-mail: cedric.beaume@imft.fr.

■ ACKNOWLEDGMENT

We thank Professor H.-C. Chang for helpful discussions.

■ REFERENCES

(1) Chen, C. H.; Lin, H. L.; Lele, S. K.; Santiago, J. G. Electro-kinetic microflow instability with conductivity gradients. In *Proceedings of the 7th International Conference on Micro Total Analysis Systems*, Vol. 1; Northrup, M. A.; Jensen, K. F.; Harrison, D. J., Eds.; Kluwer: Dordrecht, 2003.

(2) Chang, M. H.; Homsy, G. M. *Phys. Fluids* **2005**, *17*, 074107.

(3) Levich, V. *Physico-chemical Hydrodynamics*; Prentice Hall: Upper Saddle River, NJ, 1962.

(4) Saville, D. A. *Annu. Rev. Fluid. Mech.* **1997**, *29*, 27–64.

(5) Lin, H.; Storey, B. D.; Oddy, M. H.; Chen, C. H.; Santiago, C. J. *Phys. Fluids* **2004**, *16*, 1922–1935.

(6) Chen, C. H.; Lin, H. L.; Lele, S. K.; Santiago, J. G. *J. Fluid Mech.* **2005**, *524*, 263–303.

(7) Suresh, V.; Homsy, G. M. *Phys. Fluids* **2004**, *16*, 2349–2356.

(8) Bazant, M. Z.; Thornton, K.; Ajdari, A. *Phys. Rev. E* **2004**, *70*, 021506.

(9) Plouraboué, F.; Chang, H.-C. *Phys. Rev. E* **2009**, *79*, 041404.

(10) Plouraboué, F.; Chang, H.-C. *Anais da Academia Brasileira de Ciências* **2010**, *82*, 95–108.

(11) Singer, A.; Norbury, J. *SIAM. J. Appl. Math.* **2009**, *70*, 949–968.

(12) Neu, J. C. *Phys. Rev. Lett.* **1999**, *82*, 1072–1074.

(13) Lyklema, J.; Duval, J. F. *Adv. Colloid Interface Sci.* **2005**, *114−115*, 27–45.

(14) Chan, D. Y.; Healyb, T. W.; Supasitia, T.; Usuic, S. *J. Colloids Interface Sci.* **2006**, *296*, 150–158.

(15) Zhmud, B. V.; Meurk, A.; Bergström, L. *Colloids Surf., A* **2000**, *164*, 3–7.

(16) Biesheuvel, P. M. *Langmuir* **2001**, *17*, 3553–3556.

(17) Basu, S.; Sharma, M. M. *J. Colloids Interface Sci.* **1994**, *165*, 355–366.

(18) Lau, A. W. C.; Pincus, P. *Phys. Rev. E* **2002**, *66*, 041501.

(19) Zohar, O.; Leizerson, I.; Sivan, U. *Phys. Rev. Lett.* **2006**, *96*, 177802.

(20) Kokkoli, E.; Zukoski, C. F. *Langmuir* **1998**, *14*, 1189–1195.

(21) Sotres, J.; Baró, A. M. *Biophys. J.* **2010**, *98*, 1995–2004.

(22) Squires, T. M.; Bazant, M. Z. *J. Fluid Mech.* **2004**, *509*, 217–252.

(23) Stern, O. Z. *Elecktrochemistry* **1924**, 30.

(24) Mangelsdorf, C.; White, L. R. *J. Chem. Soc., Faraday Trans. 2* **1990**, *86*, 2859–2870.

(25) Healy, T. W.; White, L. R. *Adv. Colloid Interface Sci.* **1978**, *9*, 303–345.

(26) Baldessari, F. *J. Colloids Interface Sci.* **2008**, *325*, 526–538.

(27) Haydon, D. A. *Proc. R. Soc. London, Ser. A* **1960**, *258*, 319–328.

(28) Jiang, Z.; Stein, D. *Langmuir* **2010**, *26*, 8161–8173.

(29) Koopal, L. K.; Avena, M. J. *Colloids Surf.* **2001**, *192*, 93–107.

(30) Doedel, E. J.; Oldeman, B. E. *AUTO-07p: Continuation and bifurcation software for ordinary differential equations*; Concordia University: Montreal, Canada, 2007.

(31) Deville, M. O.; Fischer, P. F.; Mund, E. H. *High-order Methods for Incompressible Fluid Flow*; Cambridge University Press: New York, 2002.

(32) Ghzaoui, A. E. *J. Appl. Phys.* **1999**, *86*, 5894–5897.

(33) Kilic, M. S.; Bazant, M. Z.; Ajdari, A. *Phys. Rev. E* **2007**, *75*, 021502.

(34) Chu, K.; Bazant, M. Z. *SIAM. J. Appl. Math.* **2005**, *65*, 1485–1505.

(35) Wang, X.; Zhi, L.; Müllen, K. *Nano Lett.* **2008**, *8*, 323–7.

(36) Khan, U.; Porwal, H.; O'Neill, A.; Nawaz, K.; May, P.; Coleman, J. N. *Langmuir* **2011**, *27*, 9077−9082.

(37) Coleman, J. N. *Science* **2011**, *331*, 568–571.